NANO LETTERS

2007
Vol. 7, No. 4
1010−1012

Orientations of Overdamped Magnetic Nanorod-Gyroscopes

Prajnaparamita Dhar,[†] Cheryl D. Swayne,[†] Thomas M. Fischer,*[,†] Timothy Kline,[‡] and Ayusman Sen[‡]

Department of Chemistry and Biochemistry, The Florida State University, Tallahassee Florida 32306-4390, and Department of Chemistry, Pennsylvania State University, University Park, Pennsylvania 16802

Received January 19, 2007; Revised Manuscript Received March 8, 2007

ABSTRACT

Overdamped magnetic nanorod-gyroscopes driven by a rotating magnetic field undergo a series of reorientations when sedimenting on top of a surface in a viscous liquid. By changing the amplitude and the rotation frequency of the driving magnetic field, the nanorod-gyroscope either synchronizes or desynchronizes with the field and rotates either around its long or short axis. The different regimes of motion are explained theoretically by coupling the nanorod-gyroscopes motion to the creeping flow equations of the surrounding fluid. It is shown that friction anisotropy plays an important role for the orientation of the nanorod-gyroscopes.

Spinning tops are macroscopic mechanical examples for the reorientation of rotating anisotropic bodies. A *sleeping* top spinning at high frequency has a stable upright orientation. The top *wakes up* upon lowering the frequency and starts precessing and nutating. The stability of sleeping tops is important for navigation and is used in the manufacture of gyroscopes. On the atomic scale, nuclear or electronic spins reorient in the presence of oscillating magnetic fields, wherein lies the foundation for NMR and ESR spectroscopy. Magnetic resonance peaks are sharp if the resonance frequency is large compared to the spin−lattice relaxation time. There is considerable effort to manufacture high-frequency NMR spectrometers using high magnetic fields to reduce the effect of damping of the spin system. *Nanorod-gyroscopes*, i.e., gyroscopes on the nanoscale, are rare[1−8] because dissipation is a major concern for their orientational stability. Upon miniaturization, the ratio of dissipation versus the driving power increases when using the same power source. One way to suppress dissipation on the nanoscale is to move from physical power sources to more energetic chemical power sources. A rich variety of molecular motor proteins has inspired nanoscientists to create artificial machines based on chemical or biochemical interactions. One example is a molecule undergoing a unidirectional $\pi/3$ intramolecular rotation around a single bond.[9] Others use successive isomerization[10] or stimuli-induced binding affinity changes in mechanically interlocked molecular rotors for the rotation.[11]

A completely different approach is to accept the dominance of thermal fluctuations and dissipation and to exploit this by using parametric ratchet potentials for the directed motion. Brownian motors,[12] molecular transport processes,[13] thermally activated transitions in a potential landscape,[14] thermal fluctuations in an optical trap,[15] parametrically modulated magnetic traps, or stochastic resonance,[16] all use the latter approach to convert fluctuations into directed motion.

Here we report on the orientation of a ferromagnetic nanorod-gyroscope in a rotating magnetic field placed on top of a solid surface in the dissipative environment of a viscous fluid. We show that the rod undergoes a series of reorientations as a function of the frequency and amplitude of the rotating magnetic field. These reorientations result from a competition between the tendency of the system to minimize the gravitational energy, the power supplied to the rod by the rotating magnetic field, and the power dissipated by the rotating rod to the viscous liquid.

Our nanorod-gyroscopes consist of transversally magnetized ferromagnetic nanorods[17] (Figure 1) of diameter $2r = 400$ nm and length $l = 2.6$ μm subdivided into segments consisting of platinum $l_{Pt} = 468$ nm followed by nickel $l_{Ni,1} = 64$ nm, gold $l_{Au,1} = 957$ nm, and nickel $l_{Ni,2} = 106$ nm and finishes with gold $l_{Au,2} = 1.021$ μm. The nickel segments of the rod have an oblate geometry ($l_{Ni} \ll r$), and they form ferromagnetic domains with a magnetization perpendicular to the rod (transversal magnetization) when exposed to NdFeB magnets with a surface field of 0.48 T. These rods have been used previously for creating autonomously moving field-guided rods that are propelled by the chemical decom-

* Corresponding author. E-mail: tfischer@chem.fsu.edu.
[†] Department of Chemistry and Biochemistry, The Florida State University.
[‡] Department of Chemistry, Pennsylvania State University.

10.1021/nl0701556 CCC: $37.00
Published on Web 03/23/2007

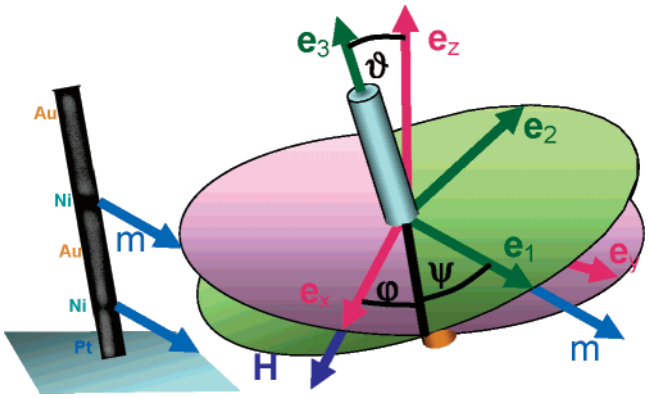

Figure 1. (left) Electron microscopy image of a magnetic nanorod-gyroscope of length 2.6 μm, showing the different nonmagnetic and magnetic segments of the rod. The rod is placed on top of a glass surface and is set into rotation by a magnetic field precessing around the surface normal. The scheme on the right shows the rod in the rest frame of the magnetic field together with the definition of the three Euler angles ϑ,φ, and ψ.

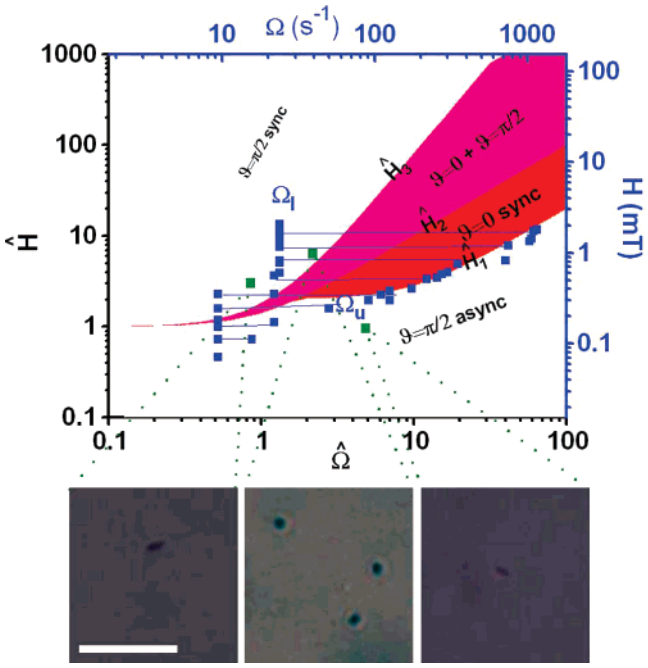

Figure 2. (top) Experimental (blue) and theoretical phase diagram for the rod orientation as a function of the precession frequency and field strength of the magnetic field. The vertical orientation of the rod is for large frequency and large magnetic field (experimental region shaded blue, theoretical region in pink and red). While theory and experiment agree in terms of the high-frequency threshold, the theoretical threshold $\hat{H}_3$ does not match the lower frequency threshold Ω_l of the experiment. We attribute this difference to the theoretical neglect of hydrodynamic interactions with the glass surface. (bottom) Microscope images of the synchronously planar, synchronously vertical, and asynchronously planar rotating rods at different frequencies and magnetic fields. The 2-D limitation to the microscope makes the rod appear as a dot if aligned vertically. Scale bar is 10 μm.

position of hydrogen peroxide at the catalytic platinum surface.[17] Here, we immerse the rods into a viscous fluid (water or glycerol water mixture) on top of a glass surface. The rods sediment in the fluid and an in-plane rotating magnetic field of frequency Ω is provided by using two coils placed perpendicular to each other. At low angular frequency, $\Omega < 9$ Hz, the rods lie on the glass surface and rotate synchronously (Figure 2 bottom left) with the magnetic field around the z-axis normal to the glass surface ($\vartheta = \pi/2$). When increasing the angular frequency, the nanorods suddenly switch orientation from a planar ($\vartheta = \pi/2$) to a vertical ($\vartheta = 0$) alignment at a threshold frequency of $\Omega_l = 9.4$ Hz. Above Ω_l, the rod rotates around its long axis (region shaded blue in Figure 2, top, and bottom middle of Figure 2). By further increasing the angular frequency, we hit a second threshold frequency Ω_u, where the rod lies down again and rotates asynchronously with an angular frequency $\omega < \Omega$ below the angular frequency of the magnetic field (Figure 2 bottom right). While the lower threshold Ω_l seems to be roughly independent of the magnetic field strength, the upper threshold monotonously increases with the magnetic field $d\Omega_u/dH > 0$. There is no vertical alignment of the rods below the minimum magnetic field $H_{min} = 56$A/m, for which the lower and upper threshold frequencies become the same $\Omega_l = \Omega_u(H_{min})$. Figure 2 summarizes our findings as a phase diagram, where we plot the rod orientation as a function of the angular frequency Ω and the magnetic field H. Both Ω_l and Ω_u decrease when we increase the viscosity by adding glycerol to the water. We have not included the glycerol/water mixture data. Although the general trend of the phase diagram for the gyroscope in the glycerol/water mixture supports our theoretical analysis outlined in the following section, the details differ and may be due to depletion effects in the stirred region. The transversal magnetization is essential for the observed reorientation behavior. Nanorods having longer (300−400 nm) nickel segments magnetize along the long rod axis and show no reorientation in a precessing field. They always exhibit planar orientation with a transition from synchronous to asynchronous rotation.

Qualitatively, we can understand the reorientation of the transversally magnetized rod as the tendency to minimize the potential energy if the system is close to static (small Ω) or if there is insufficient power supply (small H). If the system is dynamic (large Ω) and the supply of power is sufficient (large H), the system will try to minimize the entropy production and rotate around the axis of least friction that is the long axis. A more detailed understanding of the dynamics of the rod can be obtained by considering the three types of torques that are involved in the rod motion. We use two moving Cartesian coordinate systems. The first system (x,y,z) is spanned by the direction of the magnetic field (the x-direction), the y-direction, and the z-axis normal to the glass surface. The system rotates with frequency Ω with respect to the laboratory system. The second coordinate system is fixed to the rotating rod with unit vectors ($\mathbf{e}_1$, $\mathbf{e}_2$, $\mathbf{e}_3$). The unit vector $\mathbf{e}_1$ points along the magnetization of the rod and $\mathbf{e}_3$ along the long axis of the rod. A rotation matrix R(ϑ,φ,ψ) transforms the (x,y,z) system to the rod coordinate system. A magnetic torque $\tau_{magn} = \mu_0 \mu \times H$ drives the motion of the rod where μ_0 is the vacuum permittivity, μ is the magnetic moment of the rod, and $\mathbf{H} = H\mathbf{e}_x$ is the magnetic field. A

gravitational torque $\tau_g = mgl/2\ \mathbf{e}_3 \times \mathbf{e}_z$ destabilizes the upright orientation of the rod. Here m is the mass of the rod, l its length, and g the gravitational acceleration. Both torques set the rod into motion and a viscous torque $\tau_{visc} = -\eta l^3 \mathbf{k}\cdot(\omega - \Omega \mathbf{e}_z)$ counteracts the magnetic and gravitational torque, where η is the viscosity of the fluid, ω is the momentary angular frequency, and $\mathbf{k}$ is the friction coefficient tensor. If we neglect the effect of the glass surface on the hydrodynamic dissipation, the friction coefficient tensor is diagonal in the rod coordinate system with $k_{11} = k_{22} = \pi/3(\ln(2l/d) - 1.45 + 7.5(1/\ln(2l/d) - 0.27)^2)$ and $k_{33} = \pi(d/l)^2$, where d denotes the diameter of the rod.[18,19] The balance of all three torques $\tau_{magn} + \tau_g + \tau_{visc} = 0$ defines three differential equations for the three Euler angles that read:

$$\dot{\vartheta} = \sin\vartheta[1 + \hat{H}\sin\varphi\sin\psi]$$
$$\dot{\varphi} = \hat{\Omega} - \hat{H}\sin\varphi\cos\psi$$
$$\dot{\psi} = \frac{-\hat{H}[\kappa\sin\varphi\cos\psi\cos\vartheta + \cos\varphi\sin\psi]}{(1-\kappa)} \qquad (1)$$

where we have introduced the nondimensional frequency $\hat{\Omega} = 2\eta l^2 k_{11}\Omega/mg$, time $\hat{t} = mgt/2\eta l^2 k_{11}$, and magnetic field $\hat{H} = 2\mu_0\mu H/mgl$ and the friction anisotropy $\kappa = (k_{11} - k_{33})/k_{11}$, with $0 \le \kappa \le 1$. The presence of the glass surface restricts ϑ to values below $\vartheta < \pi/2$. It is straightforward to show that $\vartheta = \pi/2$, $\sin\varphi = \hat{\Omega}/\hat{H}$ is a stationary planar solution if $\hat{H} > \hat{\Omega}$. A vertical stationary solution $\vartheta = 0$, $\sin(\varphi + \psi) = -(1-\kappa)\hat{\Omega}$ to eq 1 exists if $\hat{H} > (1-\kappa)\hat{\Omega}$. In the magnetic field range between $\sqrt{1+\hat{\Omega}^2} = \hat{H}_2 < \hat{H} < \hat{H}_3 = \sqrt{(1+\kappa^2\hat{\Omega}^2)(1+\Omega^2)}$, we find a third intermediate stationary solution given by $\tan\psi = 1/\hat{\Omega}$, $\sin\varphi = \sqrt{1+\hat{\Omega}^2}/\hat{H}$, and $\cos\vartheta = -\sqrt{\hat{H}^2/(1+\hat{\Omega}^2) - 1}/\kappa\hat{\Omega}$. A linear stability analysis shows that the planar solution is stable for $\hat{H}_2 < \hat{H}$, the vertical solution is stable if $\hat{H}_2 < \hat{H} < \hat{H}_3$ or if $\sqrt{4+(1-\kappa)^2\Omega^2} = \hat{H}_1 < \hat{H} < \hat{H}_2$. The intermediate stationary solution is unstable in its entire range of validity. Hence the region $\hat{H}_2 < \hat{H} < \hat{H}_3$ is a coexistence region between planar and vertical stationary solutions, and the system relaxes to one of them. Which stationary solution is attained depends on the initial conditions. The unstable intermediate solution lies on the separatrix that separates the initial conditions relaxing into the planar position from those relaxing into the vertical position. As the intermediate stationary solution moves from $\vartheta = 0$ toward $\vartheta = \pi/2$, $\psi = \pi$, $\varphi = -\arctan(1/\hat{\Omega})$ upon lowering the magnetic field from $\hat{H} = \hat{H}_3$ to $\hat{H} = \hat{H}_2$, the catchment area of initial conditions for the vertical stationary solution continuously increases until it covers the entire accessible region $\vartheta < \pi/2$. For $\hat{H}_1 < \hat{H} < \hat{H}_2$, the vertical stationary solution is the only stable solution. Below $\hat{H} < \hat{H}_1$ and $\hat{H} < \hat{H}_2$, the system attains an asynchronous planar solution.

Our theoretical analysis is summarized in Figure 2, where we plot the different regions as a function of $\hat{\Omega}$ and $\hat{H}$ for $\kappa = 0.8$. The coexistence region between the vertical and planar orientation is depicted in pink and the vertical phase in red. Experimental data of the magnetic rods obtained in water are overlaid the theoretical prediction. There is reasonable agreement for the experimental upper frequency threshold Ω_u and the theoretical lower magnetic field threshold $\hat{H}_1$, however, the experimental vertical phase extends much further into the region of larger magnetic fields $\hat{H}_3 < \hat{H}$ and is bound by the lower frequency Ω_l rather then the theoretically predicted $\hat{H}_3$. We attribute this to the fact that we simplified the theoretical analysis in neglecting hydrodynamic interactions between the rod and the surface. Such interactions will increase the entropy production of the rod when synchronously rotating in a planar configuration. Hence hydrodynamic interactions will destabilize the planar phase in favor of the vertical phase. Such destabilization will not occur close to $\hat{H} \approx \hat{H}_1$ because there is simply not enough power supplied by the magnetic field to keep the rod upright below $\hat{H} < \hat{H}_1$. The viscous drag sets up a phase lag between the magnetization of the rod and the magnetic field such that the magnetic torque may lift the rod into the vertical position. A quantitative description incorporating hydrodynamic interactions would depend on details such as the actual separation of the rod from the glass surface.

In summary, we are able to dynamically switch the orientation of the nanorod-gyroscope from a horizontal to a vertical position by changing the frequency and strength of the precessing magnetic field. Such dynamic switches might be useful when incorporating them into microfluidic devices. They could be used as microgates for microchannels or as microstirrers that exhibit chaotic intermittent motion when operated close to the planar to vertical transition.

Acknowledgment. We thank Tom Mallouk for providing us with nanorods.

References

(1) Esashi, M.; Ono, T.; Tanaka, S. *JSME Int. J., Ser. B* **2004**, *47*, 429.
(2) Yazdi, N.; Ayazi, F.; Najafi, K. *Proc. IEEE* **1998**, *86*, 1640.
(3) Lee, S.; Park, S.; Kim, J.; Yi, S.; Cho, D. *J. Microelectromech. Syst.* **2000**, *9*, 557.
(4) Park, K. Y.; Lee, C. W.; Oh, Y. S.; Cho, Y. H., *Sens. Actuators, A* **1998**, *64*, 69.
(5) Painter, C. C.; Shkel, A. M. *IEEE Sens. J.* **2003**, *3*, 595.
(6) Fu, L.; Miao, J. M.; Li, X. X.; Lin, R. M. *Appl. Surf. Sci* **2001**, *177*, 78.
(7) Tsuchiya, T.; Kageyama, Y.; Funabashi, H.; Sakata, J. *Sens. Actuators, A* **2001**, *90*, 49.
(8) Hwang, K. H.; Lee, K. H.; Park, G. J.; Lee, B. L.; Cho, Y. C.; Lee, S. H. *J. Micromech. Microeng.* **2003**, *13*, 8.
(9) (a) Kelly, T. R.; DeSilva, H.; Silva, R. A. *Nature* **1999**, *401*, 150−152. (b) Kelly, T. R.; Silva, R. A.; DeSilva, H.; Jasmin, S.; Zhao, Y. *J. Am. Chem. Soc*. **2000**, *122*, 6935−6949.
(10) (a) Koumura, N. L.; Zijlstra, R. W. J.; van Delden, R. A.; Harada, N.; Feringa, B. L. *Nature* **1999**, *401*, 152−155. (b) Feringa, B. L.; Koumura, N. L.; van Delden, R. A.; ter Wiel, M. K. J. *Appl. Phys. A* **2002**, *75*, 301−308.
(11) Leigh, D. A.; Wong, J. K. Y.; Dehez, F.; Zerbetto, F. *Nature* **2003**, *424*, 174−179.
(12) Astumian, R. D. *Science* **1997**, *276*, 917.
(13) Fox, R. F. *Phys. Rev. E* **1998**, *57*, 2177.
(14) McCann, L. I.; Dykman, M.; Golding, B. *Nature* **1999**, *402*, 785.
(15) Ghislain, L.; Webb, W. W. *Opt. Lett.* **1993**, *18*, 1678.
(16) Gammaitoni, L.; Hänggi, P.; Jung, P.; Marchesoni, F. *Rev. Mod. Phys.* **1998**, *70*, 223−287.
(17) Kline, T. M.; Paxton, W. F.; Mallouk, T. E.; Sen, A. *Angew. Chem., Int. Ed*. **2005**, *44*, 744−746.
(18) Broersma, S. *J. Chem. Phys.* **1960**, *32*, 1626.
(19) Broersma, S. *J. Chem. Phys.* **1981**, *74*, 6989.

NL0701556